Selective Precipitation and Concentrating of Perovskite Crystals from Titanium-Bearing Slag Melt in Supergravity Field

JINTAO GAO, YIWEI ZHONG, and ZHANCHENG GUO

Selective precipitation and concentrating of perovskite crystals from titanium-bearing slag melt in the supergravity field was investigated in this study. Since perovskite was the first precipitated phase from the slag melt during the cooling process, and a greater precipitation quantity and larger crystal sizes of perovskite were obtained at 1593 K to 1563 K (1320 °C to 1290 °C), concentrating of perovskite crystals from the slag melt was carried out at this temperature range in the supergravity field, at which the perovskite transforms into solid particles while the other minerals remain in the liquid melt. The layered structures appeared significantly in the sample obtained by supergravity treatment, and all the perovskite crystals moved along the supergravity direction and concentrated as the perovskite-rich phase in the bottom area, whereas the molten slag concentrated in the upper area along the opposite direction, in which it was impossible to find any perovskite crystals. With the gravity coefficient of $G = 750$, the mass fraction of TiO_2 in the perovskite-rich phase was up to 34.65 wt pct, whereas that of the slag phase was decreased to 12.23 wt pct, and the recovery ratio of Ti in the perovskite-rich phase was up to 75.28 pct. On this basis, an amplification experimental centrifugal apparatus was exploited and the continuous experiment with larger scale was further carried out, the results confirming that selective precipitation and concentrating of perovskite crystals from the titanium-bearing slag melt by supergravity was a feasible method.

DOI: 10.1007/s11663-016-0716-8

I. INTRODUCTION

VANADIUM-TITANIUM magnetite is a kind of iron, titanium, and vanadium multiple-element symbiotic composite ore resource in massive reserves, especially in the Panxi region of China.[1,2] So far, vanadium-titanium magnetite is mainly adopted by blast furnace ironmaking processes for refining and extracting the iron, whereas use of the vanadium and titanium resources is limited. Generally speaking, the mass fraction of TiO_2 in the raw ore is 9.0 to 12.0 wt pct, and about 53 pct of TiO_2 migrates to the iron ore concentrate after mineral processing. Then the concentrate further transforms into the vanadium-bearing hot metal and the titanium-bearing blast furnace slag containing 20.0 to 25.0 wt pct of TiO_2 during the blast furnace ironmaking process.[3,4] Nevertheless, the titanium-bearing blast furnace slag can hardly resort to the traditional separating technique resulting from the dispersed distribution of the titanium component in various mineral phases, fine grains (<10 μm), and complex interfacial combination of the titanium phase. So the slag has accumulated 70 million tons and is still increasing at a rate of 3 million tons per year.[5,6]

Fortunately, many hydrometallurgy[7,8] and pyrometallurgy[9,10] studies have been throwing light on titanium separation and comprehensive use of the titanium-bearing slag. Among these, Sui and co-workers[10,11] proposed a process of precipitation combined with physical separation to recover the titanium-bearing phase from the titanium-bearing slag. As for the precipitation process of the titanium-bearing phase from the slag melt at high temperature, Zhang *et al.*,[12] Li and Sui,[13] Sun and Jahanshahi,[4] Wang *et al.*,[11,14] and Guo *et al.*[15] considered that oxidizing the slag, appropriately increasing the slag basicity, and adding some Si-Fe, CaF_2, MnO, and Fe_2O_3 powders were beneficial for the precipitation of perovskite. When it comes to the separation process of the perovskite phase, several beneficiation methods were adopted to separate perovskite and other mineral phases from the fine-ground slag, such as the flotation process and the gravity separation process.[16,17] However, none of these conventional physical methods can effectively separate the perovskite from the titanium-bearing slag at room temperature.

According to the density difference between perovskite and other minerals,[17,18] if the separating process can be carried out at the precipitation temperature of perovskite, at which perovskite transforms into a solid particle while the other minerals remain in liquid melt, it would be beneficial for the separation of the two

JINTAO GAO and YIWEI ZHONG, Lecturers, and ZHANCHENG GUO, Professor, are with the State Key Laboratory of Advanced Metallurgy, University of Science and Technology Beijing, Beijing 100083, China. Contact email: zcguo@ustb.edu.cn
Manuscript submitted March 5, 2016.
Article published online June 13, 2016.

different phases, whereas it was not feasible to accomplish this task under the conventional conditions. Considering that supergravity technology has been successfully applied in the preparation of functionally gradient materials,[19,20] separation of solid iron from slag melt,[21,22] and removal of impurities from alloy melt,[23,24] it was possible to realize the separation of perovskite crystals from titanium-bearing slag melt in the supergravity field.

In this study, selective precipitation experiments of perovskite from the slag melt were first carried out, to determine the optimum temperature range at which greater precipitation quantity and larger crystal sizes of perovskite were obtained. Thereafter, the selective concentrating experiments of perovskite crystals from the slag melt were carried out at this temperature in the supergravity field, and the influences of the supergravity field on the concentrating behavior of perovskite crystals, and the mineral compositions and components of the samples, were investigated. On this basis, an amplification experiment centrifugal apparatus was exploited and the continuous experiment with larger scale was carried out to further examine the feasibility of the entire process.

II. EXPERIMENTAL

A. *Apparatus*

In this study, the supergravity field used in the selective concentrating experiments and the amplification experiments was generated by two different centrifugal apparatuses. As for the centrifugal apparatus used for the concentrating experiments illustrated in Figure 1, a heating furnace and a counterweight were fixed symmetrically onto the centrifugal rotor, and the distance from the centrifugal axis to the center of the sample was 250 mm. The heating furnace and counterweight were kept vertical in the stationary state and changed to the level state when the centrifugal rotor started running, which could impart a maximum angular velocity of 2500 RPM. To realize the continuous precipitation and concentrating process and further scale up the experimental scale, an amplification experimental centrifugal apparatus was exploited, as illustrated in Figure 2. A vertical heating chamber with an inner diameter of 150 mm and an inside height of 100 mm was fixed horizontally onto the centrifugal rotor, and the distance from the centrifugal axis to the center of the sample was 55 mm. When the centrifugal rotor started running, the chamber rotated therewith in the horizontal direction, which could impart a maximum angular velocity of 1000 RPM. Furthermore, the centrifugal apparatus used for concentrating experiments was heated by resistance wire for a lower temperature, while the amplification experimental centrifugal apparatus was heated by microwave field to achieve a higher temperature, and the temperatures were both controlled by a program controller with an R-type thermocouple.

B. *Material*

The naturally cooled titanium-bearing blast furnace slag from the Panzhihua Iron and Steel Corporation of China was used as the raw material. As listed in Table I, the mass fractions of TiO_2 and CaO were 23.35 and 28.64 wt pct, respectively. According to the X-ray diffraction (XRD) analysis shown in Figure 3, the mineralogical compositions included perovskite ($CaTiO_3$), pyrope ($Mg_3Al_2Si_3O_{12}$), and diopside ($Ca(Mg,Al)(Si,Al)_2O_6$).

C. *Experimental Procedure*

1. *Selective precipitation of perovskite crystals from the slag melt*

The chemical agents based on the main five compositions of the real titanium-bearing slag were well mixed, and the basicity defined as CaO/SiO_2 was adjusted from 1.13 to 1.30 by increasing the mass fraction of CaO based on the experimental results of Li and Sui[13] and Sun and Jahanshahi;[4] it was called the simulated slag and used for selective precipitation experiments of perovskite crystals from the slag melt during the cooling

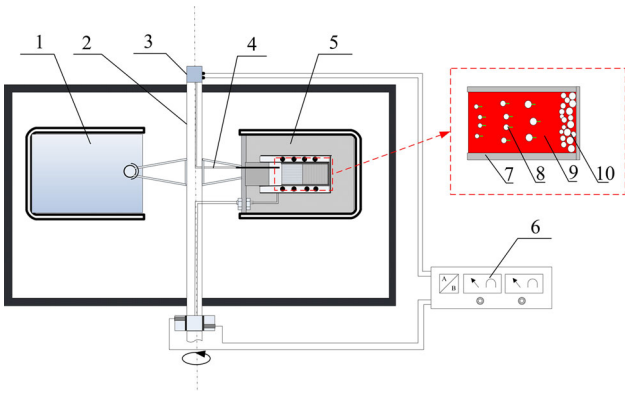

Fig. 1—Sketch of the centrifugal apparatus used for concentrating experiments: 1—counterweight, 2—centrifugal axis, 3—conductive slipping, 4—thermocouple, 5—insulating layer, 6—temperature controller, 7—graphite crucible, 8—perovskite crystals, 9—slag phase, and 10—perovskite-rich phase.

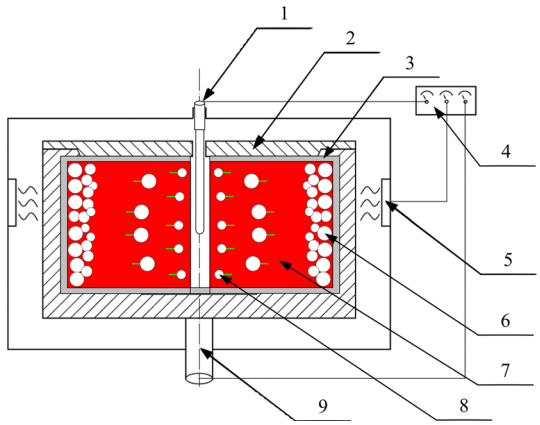

Fig. 2—Sketch of the amplification experimental centrifugal apparatus: 1—thermocouple, 2—heating chamber, 3—graphite crucible, 4—temperature controller, 5—microwave field, 6—perovskite-rich phase, 7—slag phase, 8—perovskite crystals, and 9—centrifugal axis.

process. The simulated slags were put into several molybdenum sheet–lined graphite crucibles and heated at 1773 K (1500 °C) for 30 minutes under argon gas in a muffle furnace until they were fully melted. Thereafter, the melted slags were rapidly cooled to 1743 K, 1713 K, 1683 K, 1653 K, 1623 K, 1593 K, 1563 K, 1533 K, 1503 K, 1473 K, 1443 K and 1413 K (1470 °C, 1440 °C, 1410 °C, 1380 °C, 1350 °C, 1320 °C, 1290 °C, 1260 °C, 1230 °C, 1200 °C, 1170 °C, and 1140 °C) at a cooling rate of 20 K/min (°C/min), and then the slags were slowly cooled at a cooling rate of 0.5 K/min (°C/min) from one temperature to the next. Afterward, each graphite crucible was quenched in water.

2. *Selective concentrating of perovskite crystals from the slag melt in a supergravity field*

Because the temperature of the centrifugal apparatus used for concentrating experiments was not high enough to cause the slag to melt fully, the real slag with basicity of 1.30 was first melted at 1773 K (1500 °C) and cooled slowly from 1593 K to 1563 K (1320 °C to 1290 °C) at a cooling rate of 0.5 K/min (°C/min) in the muffle furnace, and then quenched in water. Afterward, an amount of 40 g of the preceding slag was put into a graphite crucible with an inner diameter of 19 mm and heated to 1578 K (1305 °C) in the heating furnace of the centrifugal apparatus (Figure 1). Then the centrifugal apparatus was started and adjusted to an angular velocity of 1638 RPM ($G = 750$). After concentrating at 1578 K (1305 °C) for 25 minutes, the centrifugal apparatus was shut off and the graphite crucible was quenched in water. Simultaneously, the parallel experiment was carried out at the same temperature for 25 minutes in the normal gravity field.

3. *Amplification experiment*

On the basis of stepwise selective precipitation and concentrating experiments, the amplification experiment with larger scale was further carried out. An amount of 1000 g of the real slag with basicity of 1.30 was put into a graphite crucible with an inner diameter of 125 mm and an inside height of 80 mm and then covered with a graphite lid, which was heated to 1773 K (1500 °C) in the heating chamber of the centrifugal apparatus (Figure 2). After melting at a constant temperature for 30 minutes, the slag was cooled slowly at 1593 K to 1563 K (1320 °C to 1290 °C) with a cooling rate of 0.5 K/min (°C/min). Then the temperature was rapidly increased to 1578 K (1305 °C), and the centrifugal apparatus was started and adjusted to an angular velocity of 1000 RPM, namely, $G = 62$, at a constant temperature for 25 minutes. After that, the centrifugal apparatus was shut off, and the graphite crucible was quenched in water.

D. *Analytical Procedure*

In experiments (2) and (3), the gravity coefficient was calculated as the ratio of the super-gravitational acceleration to the normal-gravitational acceleration *via* Eq. [1]:

$$G = \frac{\sqrt{g^2 + (\omega^2 R)^2}}{g} = \frac{\sqrt{g^2 + \left(\frac{N^2\pi^2 R}{900}\right)^2}}{g} \qquad [1]$$

where G is the gravity coefficient, g is the normal-gravitational acceleration ($g = 9.80$ m/s^2), w is the angular velocity (rad × s^{-1}), N is the rotating speed of the centrifugal (RPM), and R is the distance from the centrifugal axis to the center of the sample.

The samples obtained by experiments (1) through (3) were sectioned longitudinally along the center axis into two parts, respectively. Then the samples were measured on a metallographic microscope (Laitz DMRX) and image analyzer (LEICA Qwin 500) by the line intercept method[25] to analyze the volume fractions and equivalent diameters of the perovskite crystals in different areas of the samples. Further, the samples obtained in the supergravity field were crossly divided along the interface into two parts and characterized by XRD (TTR III from Rigaku Corporation) and XRF (XRF-1800X from Shimadzu Corporation) to determine the mineral compositions and chemical components of the layered samples. After that, the recovery ratio of Ti was calculated *via* Eq. [2]:

$$\varepsilon_{Ti} = \frac{m_P \times \omega_{Ti-P}}{m_P \times \omega_{Ti-P} + m_S \times \omega_{Ti-S}} \times 100 \text{ pct} \qquad [2]$$

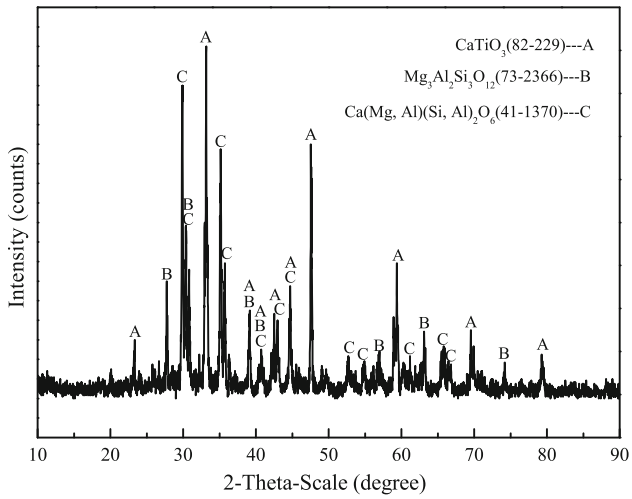

Fig. 3—XRD patterns of the titanium-bearing blast furnace slag.

Table I. Chemical Compositions (Weight Percent) of Titanium-Bearing Blast Furnace Slag and the Simulated Slag

Composition	CaO	TiO_2	SiO_2	Al_2O_3	MgO	TFe	MnO_2	V_2O_5	S	P_2O_5	Others	Basicity
Real slag	28.64	23.35	25.44	11.09	7.06	2.82	0.75	0.20	0.12	0.02	0.50	1.13
Simulated slag	33.07	23.35	25.44	11.09	7.06	—	—	—	—	—	—	1.30

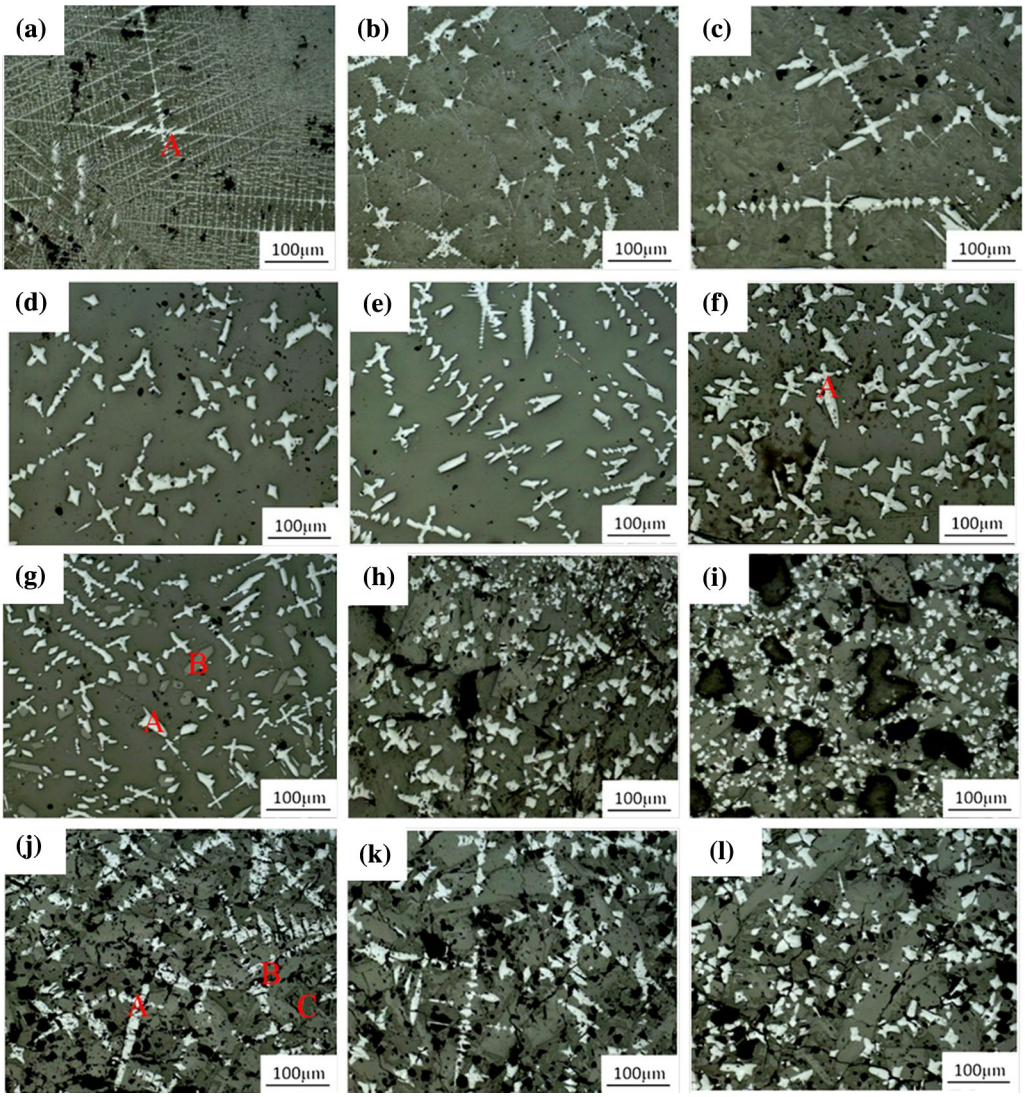

Fig. 4—Variations in microstructures of the slag melt after cooling at different temperatures: (*a*) 1743 K to 1713 K (1470 °C to 1440 °C), (*b*) 1713 K to 1683 K (1440 °C to 1410 °C), (*c*) 1683 K to 1653 K (1410 °C to 1380 °C), (*d*) 1653 K to 1623 K (1380 °C to 1350 °C), (*e*) 1623 K to 1593 K (1350 °C to 1320 °C), (*f*) 1593 K to 1563 K (1320 °C to 1290 °C), (*g*) 1563 K to 1533 K (1290 °C to 1260 °C), (*h*) 1533 K to 1503 K (1260 °C to 1230 °C), (*i*) 1503 K to 1473 K (1230 °C to 1200 °C), (*j*) 1473 K to 1443 K (1200 °C to 1170 °C), (*k*) 1443 K to 1413 K (1170 °C to 1140 °C), and (*l*) 1413 K to 1383 K (1140 °C to 1110 °C); (A) perovskite crystals, (B) pysope crystals, and (C) diopside crystals.

where ε_{Ti} is the recovery ratio of Ti in the perovskite concentrating phase; m_P and m_S are the mass fractions of the perovskite concentrating phase and slag phase, respectively; and $w_{Ti\text{-}P}$ and $w_{Ti\text{-}S}$ are the mass fractions of Ti in the perovskite concentrating phase and slag phase.

III. RESULTS AND DISCUSSION

A. *Selective Precipitation of Perovskite Crystals from the Slag Melt*

The variations in microstructures of the slag melt after cooling at different temperatures are shown in Figure 4. Combined with the variations of mineral compositions, as shown in Figure 5, it was obvious that perovskite was the first precipitated phase, and the perovskite crystals with characteristics of fine dispersing floc or spicule first appeared in the sample of 1743 K to 1713 K (1470 °C to 1430 °C), as shown in Figure 4(a). When the temperature decreased from 1713 K to 1563 K (1430 °C to 1290 °C), perovskite crystals gradually changed to larger dendrites and equiaxed crystals, as shown in Figures 4(b) through (f). When the temperature further decreased, pyrope crystals with lath shape began to precipitate at a temperature below 1563 K (1290 °C), as shown in Figure 4(g), and diopside crystals with irregular shape began to precipitate at a temperature below 1473 K (1200 °C), as shown in Figure 4(j), and uniformly distributed among the first precipitated perovskite crystals. These findings indicated that a single solid perovskite phase in a solid-liquid mixed slag only occurred at a temperature above 1563 K (1290 °C).

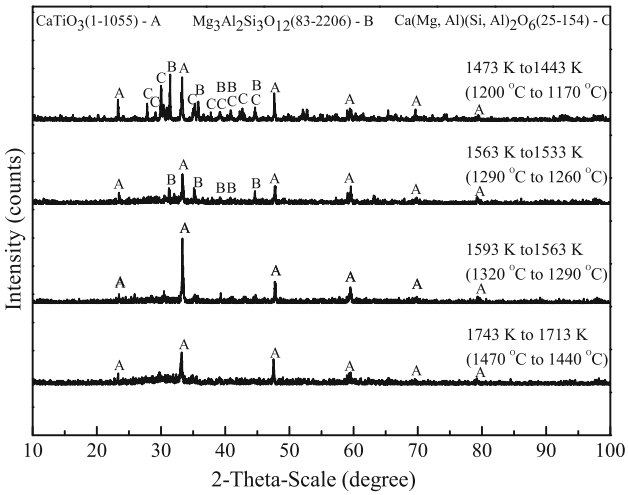

Fig. 5—Variations in XRD patterns of the slag melt after cooling at different temperatures.

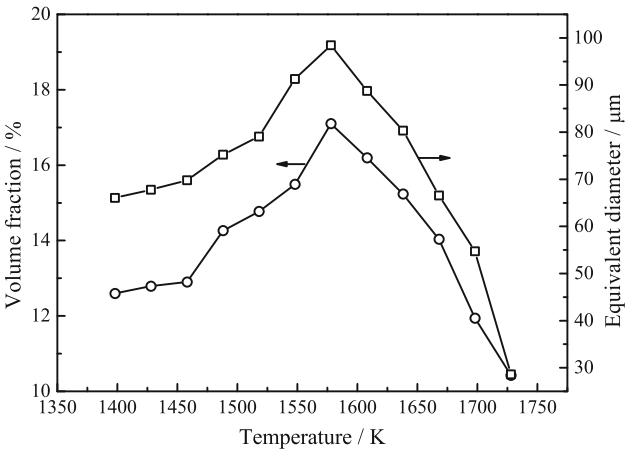

Fig. 6—Variations in volume fractions and equivalent diameters of perovskite crystals during cooling at different temperatures.

The variations in volume fraction and equivalent diameter of the perovskite crystals during cooling at different temperatures are shown in Figure 6. Obviously, they both increased first and then decreased with decreasing temperature from 1743 K to 1383 K (1470 °C to 1110 °C), and the greater precipitation quantity and larger crystal size of perovskite both appeared at 1593 K to 1563 K (1320 °C to 1290 °C). It was explained, according to the study of Eagan *et al.*,[26] that when the temperature was above 1563 K (1290 °C), only perovskite crystals existed in the melt and the migration rate of Ca^{2+} and TiO_3^{2-} in the melt was faster, which was beneficial for the nucleation and growth of perovskite crystals. However, as the temperature decreased to below 1563 K (1290 °C), the viscosity of the melt increased with the successive precipitation of pyrope and diopside, and the migration rate of Ca^{2+} and TiO_3^{2-} decreased. As a result, the nucleation and growth of perovskite crystals was blocked.

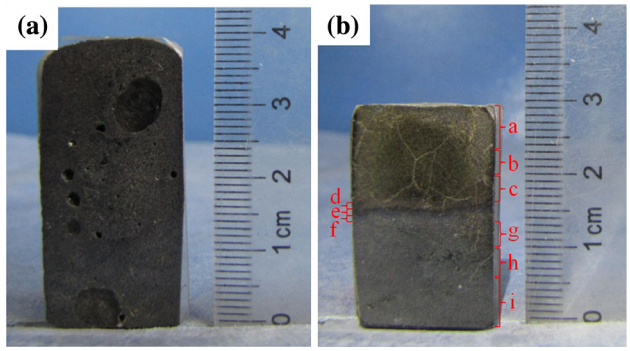

Fig. 7—Vertical sections of the sample obtained by supergravity concentrating compared with normal gravity experiments: (*a*) $G = 1$ and (*b*) $G = 750$.

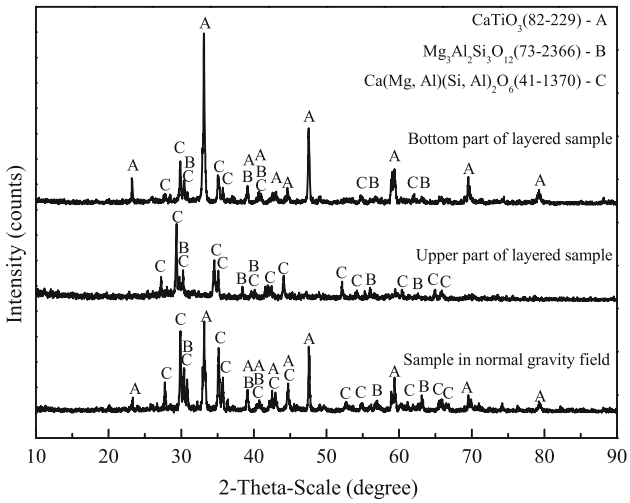

Fig. 8—XRD patterns of different areas in the layered sample obtained by supergravity concentrating experiments.

B. *Selective Concentrating of Perovskite Crystals from the Slag Melt in a Supergravity Field*

1. *Macrostructures of the samples obtained in a supergravity field*

The vertical sections of the sample obtained by supergravity concentrated with the gravity coefficient of $G = 750$ compared with normal gravity ($G = 1$) are illustrated in Figure 7. In a macroscopic view, a uniform porosity structure presented in the sample obtained in the normal gravity field. However, the layered structures appeared significantly in the sample obtained in a supergravity field. The upper part in a yellowish-gray was the glassy state, and the bottom part in a gray-white was the compact structure. Combined with the XRD analysis, as shown in Figure 8, the upper part of the layered sample was only comprised of pyrope and diopside. In contrast, the bottom part of the layered sample was mainly comprised of perovskite, and some pyrope and diopside, whereas the diffraction peak intensity of perovskite was increased while that of pyrope and diopside was reduced significantly compared with the normal gravity sample. It was evident that the other minerals transformed into molten slag and

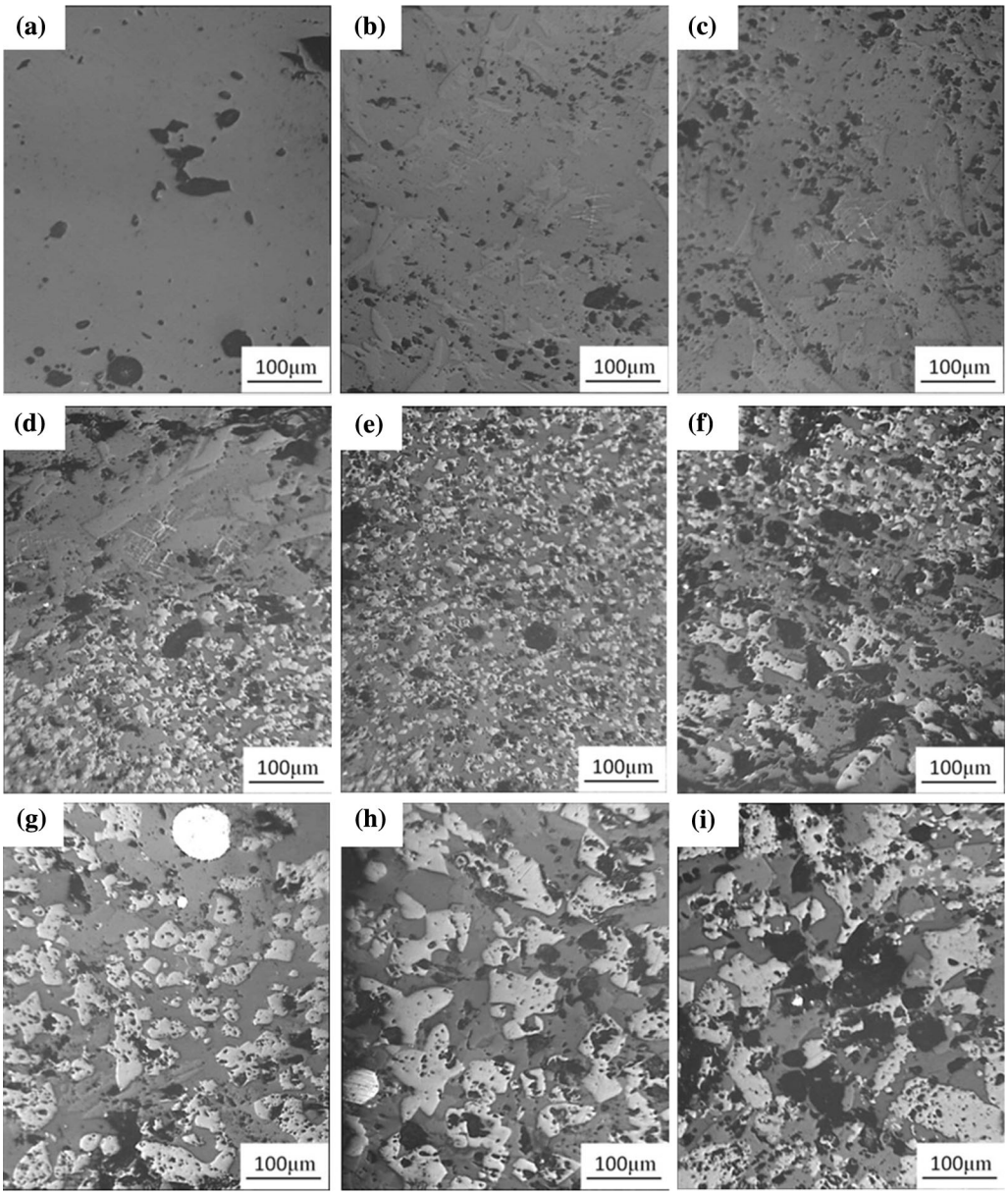

Fig. 9—Micrographs of the nine areas in the layered sample obtained by supergravity concentrating experiments: (*a*) through (*c*) the upper areas of the layered sample, (*d*) through (*f*) the interface areas of the layered sample, and (*g*) through (*i*) the bottom areas of the layered sample.

perovskite crystals remained in solid state after heating the slag to 1578 K (1305 °C), and some porosity resulted from the slow movement of perovskite crystals in the slag melt, as shown in Figure 7(a). Furthermore, the perovskite crystals moved to the bottom of the sample along the supergravity direction due to the density difference with the slag, and they concentrated as perovskite-rich phase at the bottom of the layered sample, as shown in Figure 7(b), whereas the molten slag concentrated at the top of the layered sample along the opposite direction.

2. *Concentrating behavior of perovskite crystals in a supergravity field*

To further investigate the concentrating behavior of perovskite crystals from the slag melt in the supergravity field, the layered sample was divided into nine areas along the supergravity direction, which were characterized by metallographic microscopy, as shown in Figure 9. In the upper areas (a) through (c) of the layered sample, it was practically impossible to find any perovskite crystals. Nevertheless, the fine dendrite crystals, fine equiaxed crystals, and larger equiaxed crystals of perovskite appeared successively in the upper, middle, and bottom, respectively, of the interface areas (d) through (f) in the layered sample from the top down. When it further came to the bottom areas (g) through (i) of the layered sample, the larger equiaxed crystals of perovskite appeared, and the crystal sizes increased significantly with the area approaching the bottom along the direction of supergravity.

According to the variations in volume fractions and equivalent diameters of the perovskite crystals in different areas of the layered sample, as shown in Figure 10, it was obvious that the equivalent diameters and volume fractions of perovskite crystals in the upper areas (a) through (c) were approaching zero. Instead, the equivalent diameters of perovskite crystals increased significantly from area (d) to area (i) along the supergravity direction, and the peak value appeared in the bottom area (i), which was up to 110 μm. Similarly, the volume fractions of perovskite crystals also increased from the bottom areas (g) through (i) along the supergravity direction, but the peak value presented in the interface area (e) due to the small size of perovskite crystals resulting in a great number of those accumulating in this area. It gave further evidence that all the precipitated perovskite crystals moved along the supergravity direction, collided with each other, and grew into larger equiaxed crystals; then they concentrated as the perovskite-rich phase in the bottom area of the layered sample.

3. *Components of the layered samples after supergravity concentrating*

The chemical compositions of the perovskite-rich phase and slag phase in the layered sample obtained by supergravity concentrating compared with normal gravity are shown in Table II. The mass fraction of TiO_2 in the perovskite-rich phase was up to 34.65 wt pct, whereas those of SiO_2, Al_2O_3, and MgO were decreased to 17.85, 5.97, and 4.83 wt pct, respectively. In contrast, the mass fraction of TiO_2 in the slag phase was decreased to 12.23 wt pct, whereas those of SiO_2, Al_2O_3, and MgO were up to 31.23, 15.52, and 11.37 wt pct, respectively. The supergravity field definitely was shown to be beneficial for the directional migration of perovskite crystals in the slag melt. After supergravity concentrating, an overwhelming majority of perovskite crystals were separated from the slag melt and concentrated as the perovskite-rich phase, and the recovery ratio of Ti in the perovskite-rich phase calculated *via* Eq. [2] was up to 75.28 pct.

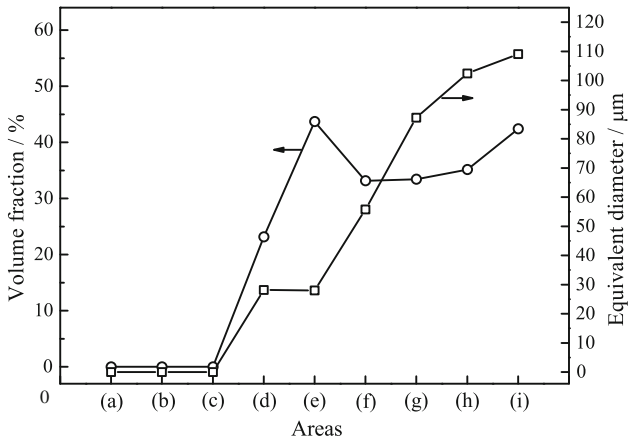

Fig. 10—Volume fractions and equivalent diameters of perovskite crystals in different areas of the layered sample obtained by supergravity concentrating experiments.

C. *Amplification Experiment*

As the cross and vertical sections of the sample obtained by the amplification experiment with the gravity coefficient of $G = 62$ shown in Figure 11, the sample was in a form of annular cylinder close to the inner wall of the crucible. The layered structures appeared significantly in the sample, with the inner part in a black glassy state and the outer part in a gray-white compact structure. Combined with the XRD analysis, as shown in Figure 12, the inner part mainly comprised of pyrope and diopside, and some perovskite, whereas the outer part mainly comprised of perovskite, and some pyrope and diopside, but the diffraction peak intensity of perovskite in the outer part increased significantly compared with that of the inner part. Furthermore, the layered sample was divided into eight areas along the supergravity direction and characterized by metallographic microscopy, as shown in Figure 13, and the volume fractions and equivalent diameters of perovskite crystals in different areas of the layered sample are

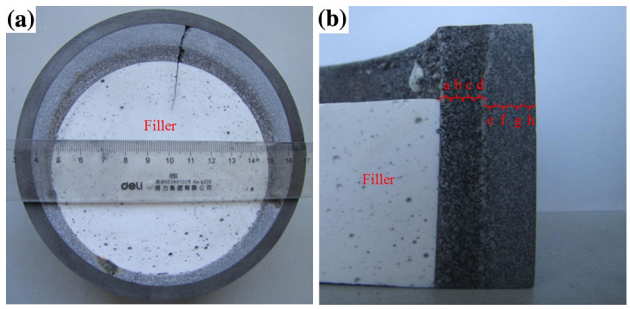

Fig. 11—Cross sections and vertical sections of the sample obtained by amplification experiments: (*a*) cross sections and (*b*) vertical sections.

Table II. Chemical Compositions (Weight Percent) of the Perovskite-Rich Phase and Slag Phase Obtained by Supergravity Concentrating Experiment

Area	CaO	TiO_2	SiO_2	Al_2O_3	MgO	Fe_2O_3
Perovskite-rich phase	34.28	34.65	17.85	5.97	4.83	2.41
Slag phase	29.01	12.23	31.23	15.52	11.37	0.64
Sample in normal gravity field	30.92	23.31	24.82	10.34	8.17	2.44

shown in Figure 14. It was obvious that only some fine networks of perovskite were found in the inner areas (a) through (c), whereas the majority of fine and larger equiaxed crystals of perovskite concentrated in the interface areas (d) through (e) and the outer areas (f) through (h), respectively. According to the chemical compositions of different parts in the layered sample as shown in Table III, the mass fraction of TiO_2 in the outer part was up to 28.07 wt pct, whereas that of the inner part decreased to 16.11 wt pct. The recovery ratio of Ti in the outer part was up to 74.96 pct. Consequently, the amplification experiment results confirmed that continuous precipitation and concentrating of perovskite crystals from the slag melt by supergravity was a feasible method; the majority of the perovskite crystals were separated from the slag melt and concentrated as perovskite-rich phase along the supergravity direction. But, due to the lower gravity coefficient obtained by the amplification experimental centrifugal apparatus, the separation effect of perovskite-rich phase and slag phase was lower than that of earlier concentrating experiments with a higher gravity coefficient.

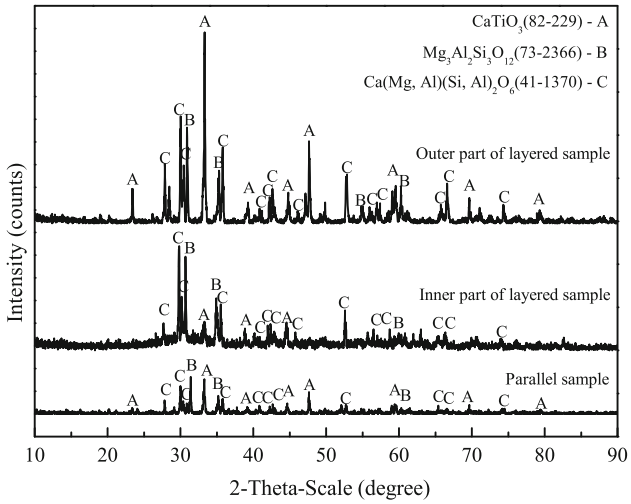

Fig. 12—XRD patterns of different areas in the layered sample obtained by amplification experiments.

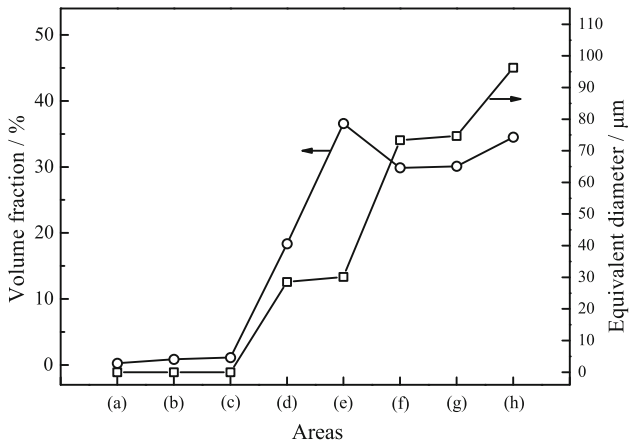

Fig. 14—Volume fractions and equivalent diameters of perovskite crystals in different areas of the layered sample obtained by amplification experiments.

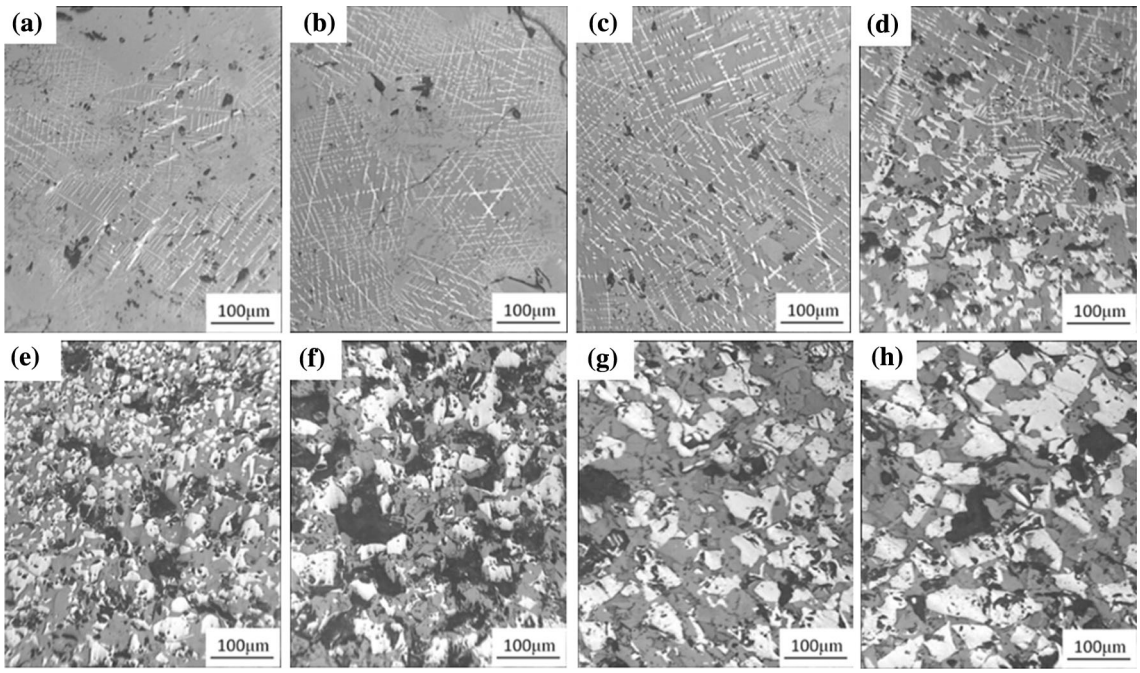

Fig. 13—Micrographs of the eight areas in the layered sample obtained by amplification experiment: (*a*) through (*c*) the inner areas of the layered sample, (*d*) and (*e*) the interface areas of the layered sample, and (*f*) through (*h*) the outer areas of the layered sample.

Table III. Recovery Ratio of Ti in the Perovskite-Rich Phase and Slag Phase Obtained by Supergravity Concentrating Experiment

Area	Mass Fraction (Pct)	Chemical Composition of TiO_2 (Wt Pct)	Recovery Ratio of Ti (Pct)
Perovskite-rich phase	51.81	34.65	75.28
Slag phase	48.19	12.23	24.72

IV. CONCLUSIONS

The selective precipitation experiment results indicated that perovskite was the first phase to precipitate from the slag melt during the cooling process, and then pryope and diopside precipitated successively at a temperature below 1563 K (1290 °C) or 1473 K (1200 °C). Furthermore, greater precipitation quantity and larger crystal size of the perovskite were obtained at 1593 K to 1563 K (1320 °C to 1290 °C).

The selective concentrating experiment results indicated that the supergravity field was definitely beneficial for the directional migration of perovskite crystals in the slag melt. After concentrating at 1578 K (1305 °C) in a supergravity field, the layered structures appeared significantly in the sample, and all the perovskite crystals moved along the supergravity direction and concentrated as perovskite-rich phase in the bottom area, whereas the molten slag concentrated in the upper area along the opposite direction. With the gravity coefficient of $G = 750$, the mass fraction of TiO_2 in the perovskite-rich phase was up to 34.65 wt pct, whereas that of the slag phase decreased to 12.23 wt pct, and the recovery ratio of Ti in the perovskite-rich phase was up to 75.28 pct.

The amplification experiment results confirmed that continuous precipitation and concentrating of perovskite crystals from the titanium-beating slag melt by supergravity was a feasible method; the majority of perovskite crystals were separated from the slag melt and concentrated as the perovskite-rich phase along the supergravity direction. However, some work on the amplification experimental apparatus and parameter is needed to further increase the separation effect of the perovskite-rich phase and slag phase in the supergravity field.

ACKNOWLEDGMENT

This study was supported by the National Natural Science Foundations of China (Grant Nos. 51404025 and 51234001).

REFERENCES

1. Z.F. Yuan, X.Q. Wang, C. Xu, W.B. Li, and M. Kwauk: *Miner. Eng*., 2006, vol. 19, pp. 975–78.
2. T. Hu, X.W. Lv, C.G. Bai, Z.G. Lun, and G.B. Qiu: *Metall. Mater. Trans. B*, 2013, vol. 44B, pp. 252–60.
3. Y. Chen, N. Yoshikawa, and S. Taniguchi: *ISIJ Int*., 2005, vol. 45, pp. 1232–37.
4. S. Sun and S. Jahanshahi: *Metall. Mater. Trans. B*, 2000, vol. 31B, pp. 937–43.
5. Y. Chen, E. Ishizuka, N. Yoshikawa, and S. Taniguchi: *ISIJ Int*., 2007, vol. 47, pp. 193–96.
6. C. Li, B. Liang, L.H. Guo, and Z.B. Wu: *Miner Eng*, 2006, vol. 19, pp. 1430–38.
7. T.A. Lasheen: *Hydrometallurgy*, 2008, vol. 93, pp. 124–28.
8. Y.J. Zhang, Q. Tao, and Y. Zhang: *Hydrometallurgy*, 2009, vol. 96, pp. 52–56.
9. Y. Morizane, B. Ozturk, and R.J. Fruehan: *Metall. Mater. Trans. B*, 1999, vol. 31B, pp. 29–43.
10. Z.T. Sui, Z.Z. Guo, L. Zhang, L.N. Zhang, M.Y. Wang, T.P. Lou, and G.Q. Li: *J. Mater. Metall*., 2006, vol. 5, pp. 93–97.
11. M.Y. Wang, L.S. Li, L. Zhang, L.N. Zhang, G.F. Tu, and Z.T. Sui: *Rare Met*., 2006, vol. 25, pp. 106–10.
12. L. Zhang, L.N. Zhang, M.Y. Wang, G.Q. Li, and Z.T. Sui: *ISIJ Int*., 2006, vol. 46, pp. 458–65.
13. L.S. Li and Z.T. Sui: *Acta Phys. Chim. Sinica*, 2001, vol. 17, pp. 845–49.
14. M.Y. Wang, L.N. Zhang, L. Zhang, Z.T. Sui, and G.F. Tu: *Trans. Nonferrous Met. Soc. China*, 2006, vol. 16, pp. 421–25.
15. Z.Z. Guo, T.P. Lou, L. Zhang, L.N. Zhang, and Z.T. Sui: *Acta Metall Sin. (Engl. Lett.)*, 2007, vol. 20, pp. 9–14.
16. L. Zhang, L.N. Zhang, M.Y. Wang, G.Q. Li, and Z.T. Sui: *Miner. Eng*., 2007, vol. 20, pp. 684–93.
17. J.W. Ma, Z.T. Sui, and B.C. Chen: *Trans. Nonferrous Met. Soc. China*, 2000, vol. 10, pp. 520–23.
18. S. Sukenaga, S. Haruki, Y. Nomoto, N. Saito, and K. Nakashima: *ISIJ Int*., 2011, vol. 51, pp. 1285–89.
19. M.R. Rahimipour and M. Sobhani: *Metall. Mater. Trans. B*, 2013, vol. 44B, pp. 1120–23.
20. T.P.D. Rajan, R.M. Pillai, and B.C. Pai: *Int. J. Cast. Met. Res*., 2008, vol. 21, pp. 214–18.
21. J.T. Gao, Y.W. Zhong, L. Guo, and Z.C. Guo: *Metall. Mater. Trans. B*, 2016, vol. 47B, pp. 1080–92.
22. J.T. Gao, L. Guo, and Z.C. Guo: *ISIJ Int*., 2015, vol. 55, pp. 2529–36.
23. L.X. Zhao, Z.C. Guo, Z. Wang, and M.Y. Wang: *Metall. Mater. Trans. B*, 2010, vol. 21B, pp. 505–08.
24. L.X. Zhao, Z.C. Guo, Z. Wang, and M.Y. Wang: *Metall. Mater. Trans. A*, 2010, vol. 21A, pp. 670–75.
25. M. Nyoka, G. Akdogan, R.H. Eric, and N. Sutcliffe: *Metall. Mater. Trans. B*, 2003, vol. 34B, pp. 833–42.
26. R.J. Eagan, J.P. Luca, and C.G. Bergeron: *J. Am. Ceram. Soc*., 1970, vol. 53, pp. 214–19.